Lab on a Chip

PAPER

View Article Online
View Journal

Cite this: DOI: 10.1039/c3lc51076j

Magnetoactive sponges for dynamic control of microfluidic flow patterns in microphysiological systems†

Sungmin Hong,‡[a] Youngmee Jung,‡[bc] Ringo Yen,[b] Hon Fai Chan,[b] Kam W. Leong,[b] George A. Truskey*[b] and Xuanhe Zhao*[a]

Received 21st September 2013,
Accepted 25th November 2013

DOI: 10.1039/c3lc51076j

www.rsc.org/loc

We developed a microfluidic flow-control system capable of dynamically generating various flow patterns on demand. The flow-control system is based on novel magnetoactive sponges embedded in microfluidic flow channels. Applying a non-uniform magnetic field compresses the magnetoactive sponge, significantly reducing porosity and hydraulic conductivity. Tuning the applied magnetic field can dynamically vary the flow rate in the microfluidic channel. Pulsatile and physiological flow patterns with frequency between 1 and 3 Hz, flow rates between 0.5 and 10 μL min^{-1} and duration over 3 weeks have been achieved. Smooth muscle cells in engineered blood vessels perfused for 7 days aligned perpendicular to the flow direction under pulsatile but not steady flow, similar to the *in vivo* orientation. Owing to its various advantages over traditional flow-control methods, the new system potentially has important applications in microfluidic-based microphysiological systems to simulate the physiological nature of blood flow.

Introduction

Microfluidic chips[1] have been widely used in biological and biomedical fields such as three-dimensional cell culture systems,[2] single cell analysis and sorting,[3] cell-containing microsphere generation,[4] and protein concentration analysis.[5] More recently, microphysiological systems that incorporate the key functions of individual organs and enable interactions among different microphysiological units have been successfully implemented with microfluidic systems.[6–10] These microfluidic-based microphysiological systems provide a novel platform to simulate normal and pathological functions for prolonged periods of time, representing human physiology for the evaluation of drug efficacy and toxicity. It is anticipated that the microphysiological systems will eventually enable rapid and high fidelity evaluation of safety and efficacy for various candidate therapeutics.

In order to accurately represent human physiology, it is critical to simulate blood flow patterns in the microfluidic chips of microphysiological systems. For example, physiological pulsatile pressure causes blood vessels to stretch[11] and the mechanical stress generated by the pulsatile flow affects the function of vascular cells.[12–16] Despite the importance of physiological flows in microphysiological systems, it has been generally challenging to dynamically control flows in microfluidic chips, due to the lack of tunable pumps with suitable dynamic response, the potential of contamination, and the difficulty of generating physiological shear stress for periods ranging from hours to days.[17]

Existing microfluidic flow-control mechanisms can be generally divided into two major categories based on methods that use deflection of flexible membranes[17–23] or external pressure pumps,[24,25] respectively. The flexible-membrane-deflection method uses mechanical forces, such as those from piezoelectric pin, magnetic disc, or high-pressure compressed air, to deform a thin membrane to seal the channel and thereby stop the flow. However, this method usually creates only on–off flow patterns, and requires relatively complicated fabrication processes such as multiple-layer assembly. As an alternative method, the pressure-pump systems control flow patterns with external pressure pump connected to a set of solenoid valves, an air compressor, a function generator, and a pressure controller.[23,24] Although the pressure-pump systems can dynamically control flow patterns, applications have been limited due to the complex system configurations and high cost of external supporting equipment. Furthermore, it is not clear whether the pressure-

[a] *Soft Active Materials Laboratory, Department of Mechanical Engineering and Material Science, Duke University, Durham, NC 27708-0287, USA. E-mail: xuanhe.zhao@duke.edu*

[b] *Biomedical Engineering Department, Duke University, Durham, NC 27708-0287, USA. E-mail: gtruskey@duke.edu*

[c] *Korean Institute of Science and Technology (KIST), Seoul, Korea*

† Electronic supplementary information (ESI) available. See DOI: 10.1039/c3lc51076j

‡ These authors contributed equally.

pump systems can generate complicated physiological flow patterns for microphysiological systems, such as a reverse flow during diastole stage of heart beating.

Here, we demonstrate a simple yet effective method to dynamically control microfluidic flows with a wide variety of rates, frequencies and patterns required by microphysiological systems based on novel magnetoactive sponges.[26–28] The magnetoactive sponge is embedded as a tunable valve across the microfluidic channel (Fig. 1a). A non-uniform magnetic field is applied on the magnetoactive sponge by simply approaching a bar of magnet to the sponge. The magnetic field compresses the magnetoactive sponge, significantly changing its porosity and therefore hydraulic conductivity. As a result, the flow rate in the channel can be dynamically varied by tuning the magnetic field applied on the sponge. Owning to its simple and low-cost fabrication, fast response, and versatility in controlling microfluidic flows, the new flow-control mechanism based on magnetoactive sponges will potentially find important applications in various microphysiological systems.

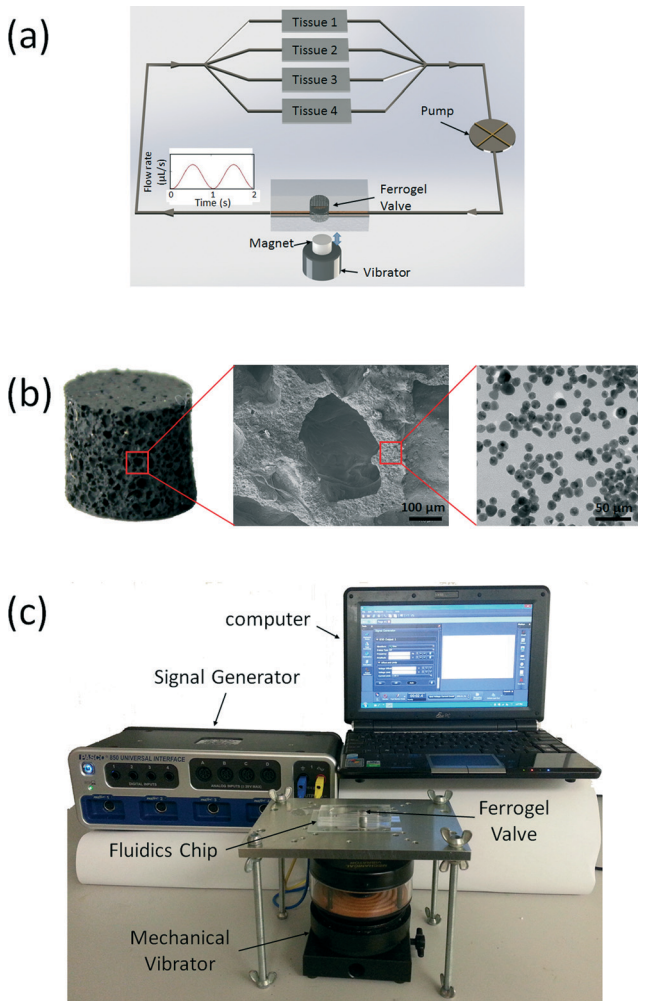

Fig. 1 (a) The schematic diagram of the configuration of fluidic system. (b) The photograph of porous sponge (left), the SEM image of pore (middle) and the TEM image of dispersed iron powder (right). (c) A photograph of the flow control system.

We also show the effect of pulsatile flow on the response of engineered blood vessels.

Materials and methods

Fabrication of magnetoactive sponge and microfluidic control device

Polydimethylsiloxane (PDMS) prepolymer and curing agent (Sylgard 184, Dow Corning) were mixed by a weight ratio of 20 : 1. Thereafter, carbonyl-iron powders (Sigma-Aldrich Co., St. Louis, MO) with diameters of 6–9 μm and brown sugar particles with diameters of 100–500 μm were added into the pre-cured PDMS solution and mixed thoroughly. The weight ratio of PDMS, iron powder, and sugar in the resultant mixture was 1 : 3 : 3. After curing the PDMS mixture at 80 °C overnight, it was cut into cylinders with height of 5 mm and diameter of 7 mm, which were then placed in deionized water overnight to dissolve the sugar particles.[26–28] The dissolution of the sugar particles produced interconnected pores in the elastomer, giving a magnetoactive sponge with carbonyl-iron powders embedded in PDMS. Thereafter, the cylinders of magnetoactive sponge were dried and installed in the flow control unit. The flow control device was fabricated by constant-volume-injection method[29,30] to give channels with height of 1.5 mm and width of 1 mm. A cylindrical chamber was fabricated across the channel to host the magnetoactive sponge (see ESI† for detail fabrication procedure).

System setup for the control of flow pattern

The desired flow patterns were generated by compressing the magnetoactive sponge with a varying magnetic field to change the porosity and hydraulic permeability of the sponge. A neodymium magnet (D76, K&J Magnetics, Inc., Pipersville, PA) with a surface magnetic field of 5071 Gauss (diameter 7/16" and height 3/8") was used to remotely compress the magnetoactive sponge to various strains by varying the distance between the magnet and the sponge. The magnet was installed on top of a mechanical vibrator (SF-9324, PASCO, Roseville, CA) that oscillated vertically. A signal generator (UI-5000, PASCO, Roseville, CA) was connected to the mechanical vibrator to control its movements through input signals from a computer (Fig. 1c).

Analysis of flow patterns

Flow patterns in the fluidic channels were analyzed using the particle tracking method.[31] Polystyrene microspheres (Polysciences Inc., Warrington, PA) with diameter of 6 μm were dispersed in DI water. Tygon silicone tubing (OD: 3/32", ID: 1/32") was used to connect the inlet of the channel to a 3 mL syringe preloaded with water/microspheres solution. A syringe pump delivered the fluid to the channel. The fluid was allowed to fill the channel and outlet port to avoid wetting effects. The mechanical vibrator was oscillated at

frequencies between 1–3 Hz (Fig. 2a). An inverted microscope (Nikon LV 100) with 20× objective lens (Numerical Aperture: 0.35) was used to record polystyrene microsphere locations over time. The motion of microspheres was recorded at a rate of 30 frames per second by a CCD camera. In order to analyze the flow velocity, the recorded video was extracted at 0.1 second intervals. The moving distance was analyzed by measuring the pixels traveled by the particle from each image (Fig. 2b) and flow velocity was obtained by calculating the moving distance per unit time (Fig. 2c). The obtained data points of flow velocity were fitted to nonlinear Lorentz curve fitting function.

Evaluation of the effect of different flow patterns for the tissue engineered blood vessels

To study the effect of different flow patterns in the physiological system, tissue engineered blood vessels (TEBVs) in a perfusion bioreactor were connected to the microfluidic control device. To prepare the TEBVs, dense collagen gels were produced from type I collagen solution from rat-tail tendon (2.05 mg ml^{-1}, BD Biosciences) and human bone marrow derived mesenchymal stem cells (hMSCs) were incorporated into the neutralized collagen solution at an average density of 2×10^5 cells ml^{-1}. After gelation at 37 °C, dense collagen sheets were produced by applying an unconfined compressive stress of 1 kPa for 5 min.[13] TEBVs were generated by rolling the dense collagen sheet along the long axis of a stainless steel mandrel (2 mm diameter).[13] After these TEBVs were connected to the perfusion chamber (KISTECH, Korea), human peripheral blood derived endothelial progenitor cells (5×10^5 cells per vessel) were seeded into the vessel and the chamber was rotated for 30 min with 0.17 rpm in the incubator. Then, perfusion chambers were connected to the peristaltic pump (MasterFlex® L/S®, Model 7550-50, Cole-Parmer, IL) with Tygon tubing. The pump supplied a steady flow (2 ml min^{-1}) with microfluidic control device and the chamber was placed in the 5% CO_2 incubator for 7 days at 37 °C.

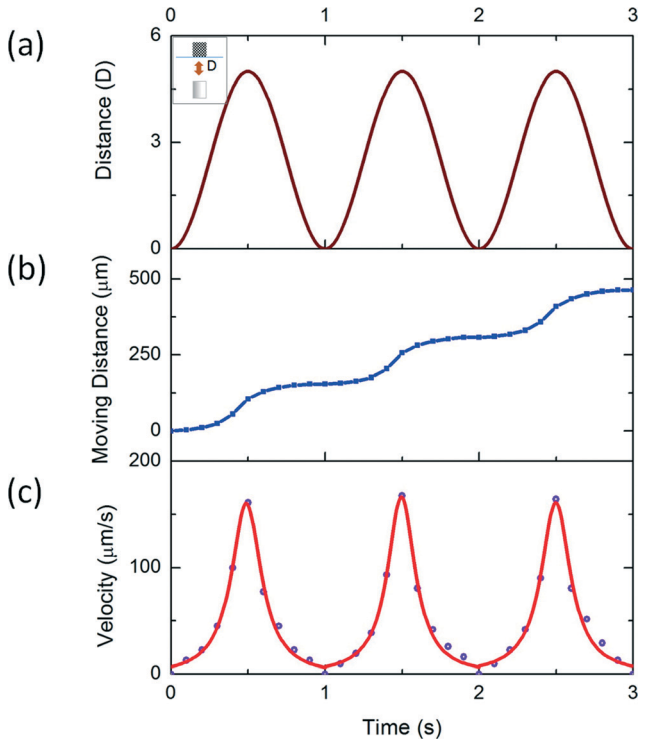

Fig. 2 Method for generating flow patterns. (a) The distance between magnet and magnetoactive sponge as a function of time. (b) Representative plot of particle movement *vs.* time at 1 Hz frequency. (c) Particle velocity profile (solid points) and its fitting curve.

To observe the distribution of vascular extracellular matrix and cellular alignment by different flow patterns, immunofluorescence staining was performed. TEBVs were fixed with 4% paraformaldehyde in PBS for 24 h at room temperature, and permeabilized in a blocking solution, which consisted of 0.03 g ml^{-1} bovine serum albumin (BSA, Sigma) and 0.1% goat serum (Sigma) in 0.2% Triton X-100 (Sigma) in PBS for 2 h. Type IV collagen and laminin were stained by using anti-type IV collagen antibody (1 : 200; Abcam, Cambridge, MA) and anti-Laminin antibody (1 : 200; Abcam), respectively, followed by the Alexa Fluor 594 goat anti-rabbit secondary antibody (1 : 200; Invitrogen, Carlsbad, CA), respectively. Also, the cell nuclei were stained with 4,6-diamidino-2-phenylindole (DAPI, Molecular Probes). After immunostaining, the samples were then mounted in Fluoro-Gel (Electron Microscopy Sciences, Hatfield, PA) for fluorescent imaging and viewed with a Zeiss LSM 510 inverted confocal microscope. Then, fluorescence images were analyzed using ImageJ for examining the cell alignment by different flow patterns, following a previously published protocol.[32] From the analysis of images, the nuclear area, major and minor axes, and angle between the major axis and the reference direction were then computed. The alignment angles and elongation aspect ratio were calculated accordingly.

The biological activity of TEBVs was evaluated after TEBVs were cultured for 7 days with different flow patterns. For examining the response of TEBV for the vasoconstrictor, the chamber connected with TEBVs was placed on a microscope stage (SM3-TZ, Amscope, CA), connected to a video camera and computer with ImageJ software, perfused with a culture media. Vessel diameters were measured before and after perfusion with the vasoconstrictor phenylephrine (1 μM). Media samples were taken to measure nitric oxide (NO) release. Medium samples were frozen at −80 °C and lyophilized (Appropriate Technical Resources, Laurel, MD) for 24 h. The lyophilized medium was resuspended into 1/10 of its original volume in double-distilled water (ddH_2O), and mixed with equal volumes of 1× Greiss Reagent (Sigma) and sample in 96 well plates (BMG Labtech, Ortenberg, Germany). Spectrophotometric absorbance was measured at 540 nm after 15 min. A standard curve was prepared using 0 to 80 μM sodium nitrite solutions in ddH_2O. The values were analyzed by one-way analysis of variance (ANOVA), followed by non-parametric LSD tests. A $p < 0.05$ was considered to indicate statistical significance.

Results and discussion

The temporal flow patterns in the microfluidic channel are controlled by changing the hydraulic permeability of magnetoactive sponge, which is tuned by varying the sponge's pore sizes under compressive strain. The compressive strain in the magnetoactive sponge is induced by the non-uniform magnetic field from the magnet. The applied magnetic field and compressive strains in the magnetoactive sponge are controlled by varying the distance between the magnet and sponge. When the magnet is far away from the sponge (*e.g.*, 5 mm), the sponge is undeformed and maintains its as-fabricated pore size (Fig. 3a), giving relatively high hydraulic permeability (Fig. 3g). (See ESI† for the measurement of hydraulic permeability.) As the distance between magnet and sponge decreases, the sponge is gradually compressed, closing its pores and reducing its hydraulic permeability (Fig. 3b). As the magnet reaches the bottom surface (less than 1 mm) of the control unit (Fig. 3c), the compressive strain in the sponge reaches 37% of its maximum value and the fluid flow in the channel is fully stopped, due to negligible hydraulic permeability of the deformed sponge with closed pores. The SEM images in Fig. 3d–f demonstrate the variation of pore sizes in the sponges under various levels of compressive strains. Furthermore, when the compressed sponge is suddenly relaxed, the flow control unit can even induce a reverse flow, due to the pressure drop in the sponge chamber.

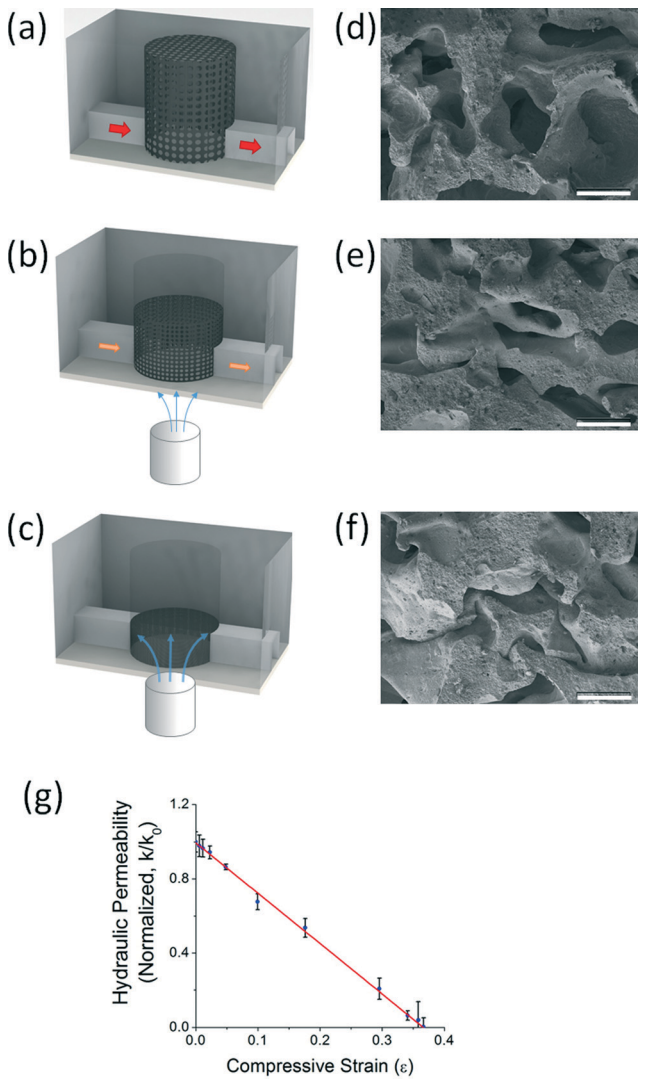

Fig. 3 The working mechanism of the magnetoactive sponge. (a)–(c) The schematic diagram that showed the change of pore size by applying magnetic field. (d)–(f) SEM image of pore size: (d) without magnetic field, (e) at 2.5 mm distance between magnet and sponge, (f) when magnet is fully contacted to sponge(scale bar: 200 μm). (g) A plot of normalized hydraulic permeability as a function of applied strain.

Now, we demonstrated the capability of magnetoactive-sponge-based microfluidic system in generating various temporal flow patterns. We first generated pulsatile flow patterns at a frequency of 1 Hz for flow rates ranging from 0.5 μL min^{-1} to 10 μL min^{-1} by the syringe pump. The distance between the magnet and sponge is prescribed to follow a pulsatile function of 1 Hz in all cases. Deionized water with microspheres flows into one end of control channel (with sponge), and an observation channel (without sponge) is connected to the other end of the control channel by silicone tubing to demonstrate the follow patterns. Video S1† qualitatively demonstrates the undulation of flow velocity in the microfluidic channel, and Fig. 4a gives quantitative results of the flow-velocity profiles. From the results, it is clear that the magnetoactive-sponge based system is able to generate pulsatile flow patterns with frequency of 1 Hz and flow rates in the range of 0.5 to 10 μL min^{-1}. Furthermore, the pulsatile flow patterns generated by the system are stable over 3 weeks. (See ESI† for long term test.) The Hartmann number (Ha) is calculated to estimate the magnetohydrodynamic effects on this system.[33] The Ha for DI water increases from 0 to 1.76×10^{-3} as the magnet approaches to the fluidic channel, and from 0 to 1.08 for tissue culture media. Since the Ha numbers for both DI water and culture media under maximum magnetic field are relatively low, it is expected that the magnetohydrodynamic effect is relatively insignificant compared with the effect of permeability variation of the sponge under magnetic field. Furthermore, we applied magnetic field to microfluidic channels with DI water and tissue culture media but without the magnetoactive sponge, and we observed insignificant variation of the flow pattern.

The resting heart rate is about 60 to 80 beats per minute (bpm, equivalent to 1 to 1.33 Hz) in normal adult human, and about 30 bpm (equivalent to 0.5 Hz) in highly trained endurance athletes.[34] On the other hand, the embryonic heart rate measures up to 155 bpm (equivalent to 2.58 Hz).[35] Therefore, flow patterns with a wide range of frequencies are necessary to mimic the physiological condition in different scenarios. By tuning the input signal from the signal generator, the magnet is able to oscillate with different frequencies in the range of 0.5 to 3 Hz and the magnetoactive sponge varies its hydraulic permeability accordingly. As shown in Fig. 4b and Video S2,† the flow patterns in the microfluidic channel are

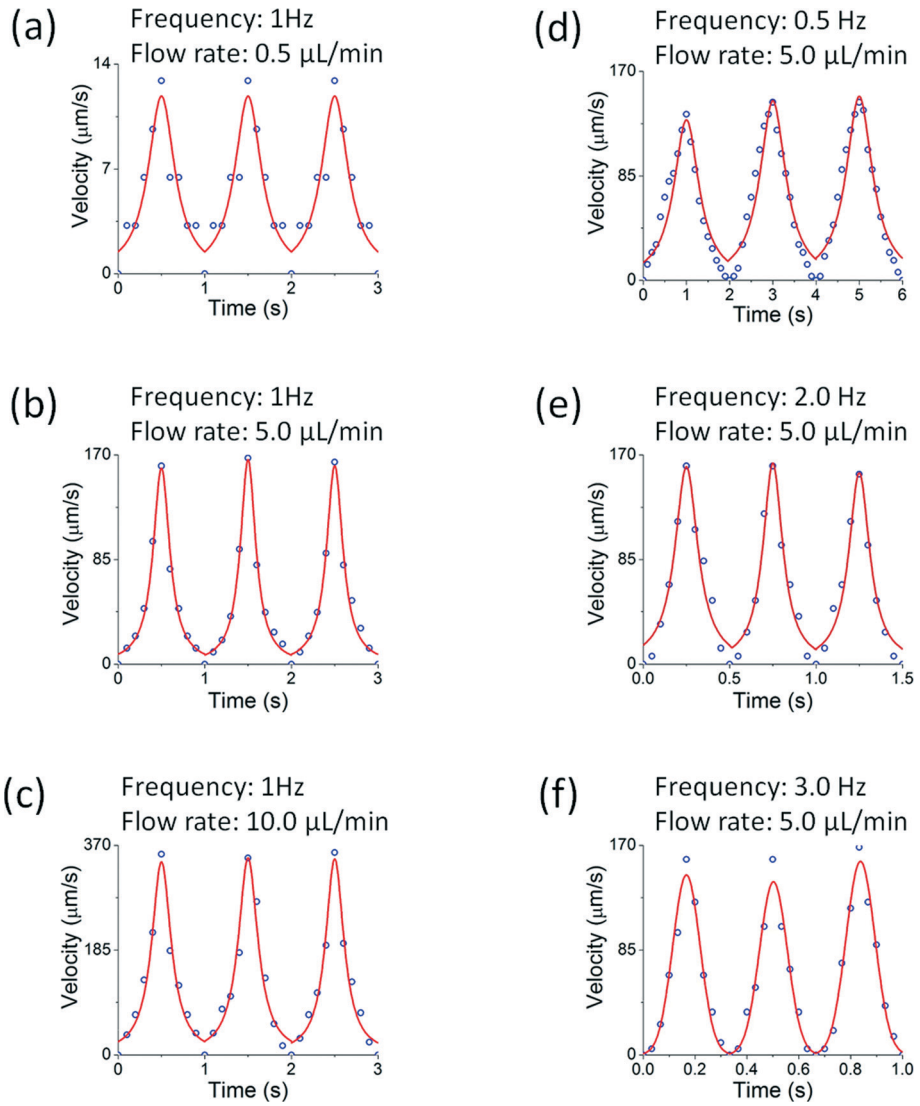

Fig. 4 Flow pattern analysis at the various conditions. (a)–(c) The pulsatile particle velocity patterns at flow rates of (a) 0.5 μL min^{-1}, (b) 5.0 μL min^{-1}, and (c)10.0 μL min^{-1} with 1 Hz frequency. (d)–(f) The pulsatile particle velocity patterns with different frequencies of (d) 0.5 Hz, (e) 2 Hz, and (f) 3 Hz at flow rate of 5.0 μL min^{-1}.

well controlled according to the input signal with frequencies ranging from 0.5 to 3 Hz.

Since the aortic valve is closed during *diastole*, blood is not allowed to flow, resulting in flow velocity leaving the heart going to zero and then making a pulsatile flow during *systole*.[36] While implementation of the physiological flows is critical for microphysiological systems, it is challenging to generate such complicated flow patterns with conventional microfluidic chips. A major advantage of the magnetoactive-sponge-based microfluidic system is its capability of generating complicated user-defined flow patterns. To achieve the physiological cardiac flow patterns, we prescribe the distance between the magnet and sponge to follow the pattern shown in Fig. 5a by programming the input signal to control the mechanical oscillator. When the magnet stays at the closest position to the magnetoactive sponge, the pores in the sponge are closed and the flow is fully stopped. Thereafter, the pores are opened as the magnet moves away from sponge, generating a pulsatile flow. Fig. 5b and Video S3† give the resultant flow pattern generated by the magnetoactive-sponge-based microfluidic system.

Spronk *et al.* measured the blood waveform at the common femoral artery using ultrasound scanning.[37] They categorized four types of waveform: triphasic, biphasic, sharp monophasic, and poor (blunted) monophasic. Triphasic and biphasic waveforms have sharp systolic forward flow as well as reverse flow during diastole whereas other waveforms have not. They also indicated that the poor monophasic waveform was found in case of aortoiliac obstructive disease. Therefore, mimicking the forward and backward flows is critical for physiological flow patterns in microphysiological systems. As shown in Fig. 5b, the flow pattern generated by the magnetoactive sponge can give both forward and reverse flow, consistent with the blood flow pattern in physiological conditions.

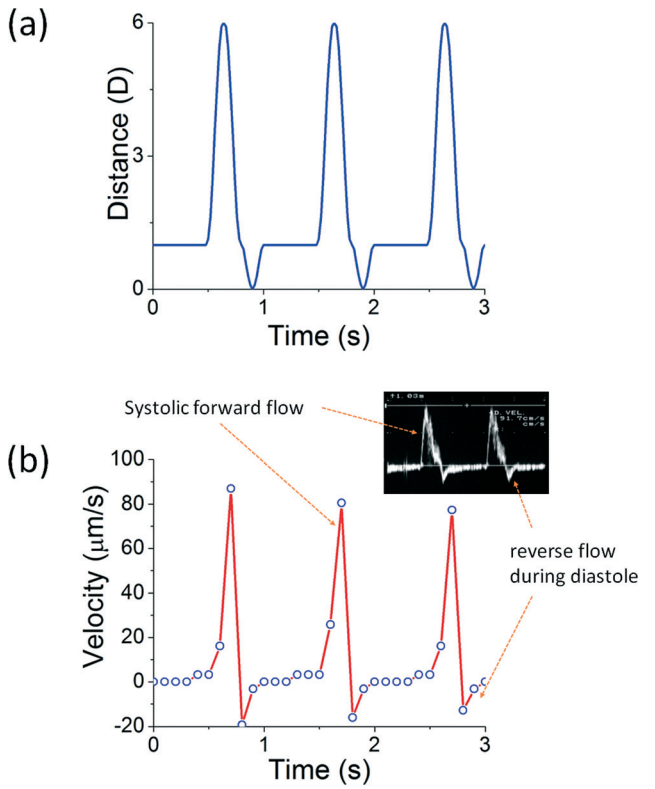

Fig. 5 Generation of physiological flow pattern. (a) Prescribed distance between the magnet and magnetoactive sponge as a function of time. (b) Measured physiological flow pattern. (Inset: ultrasound scan of typical biphasic blood waveform at common femoral artery[37]).

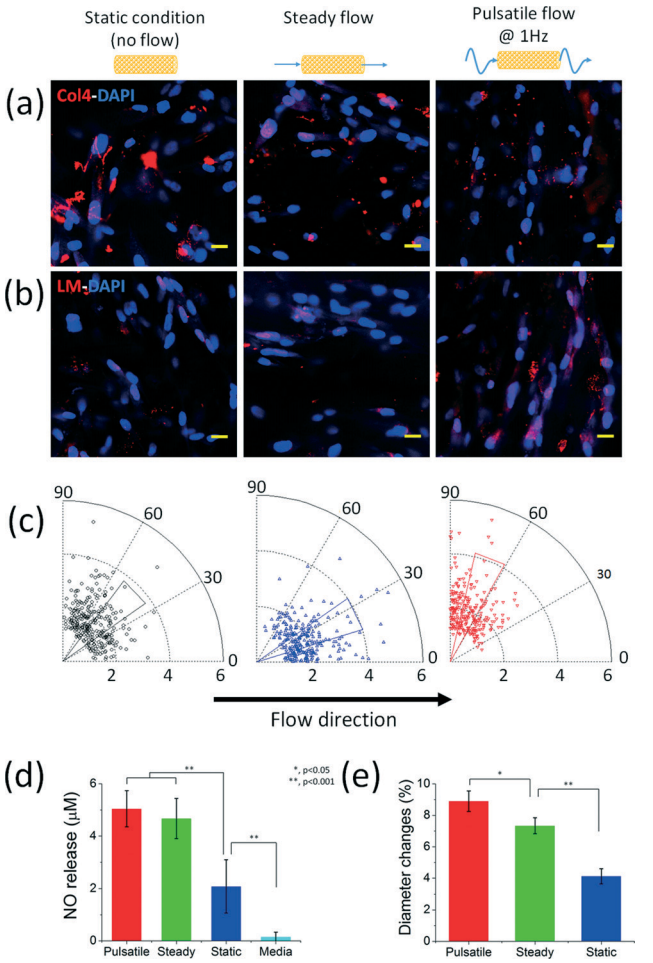

Fig. 6 Analysis of the effects of flow patterns on TEBV. (a) Confocal microscope images of collagen IV and nuclear alignment under different flow patterns. Scale bar: 20 μm. (b) Confocal microscope images of laminin and nuclear alignment under different flow patterns. Scale bar: 20 μm. (c) The polar plots of measured nuclear alignment angles under different flow patterns. (d) NO release rate under different flow patterns. (e) Vasoconstriction in response to 1 μM phenylephrine under different flow patterns.

As a test of the system, we produced TEBV to evaluate the flow effect on mesenchymal stem cell alignment under the conditions of static, steady flow, and pulsatile flow. Liu *et al.* performed the *in vivo* study that showed smooth muscle cells (SMCs) are perpendicularly aligned under non-uniform blood flow but not under static flow.[38,39] To mimic the pulsatile flow pattern *in vivo*, a flow control unit was connected to a perfusion chamber containing the TEBV and generated the pulsatile flow for one week at 1 Hz frequency. The culture media was continuously flowed in the closed loop system by peristaltic pump and we have not observed significant fouling or occlusion of the sponge by tissue culture media with proteins over 7 days. Steady flow samples were exposed to a constant flow rate of 2 ml min^{-1} for one week and static flow vessel was cultured for one week in the media without any flow. Fig. 6a–b shows the confocal microscopic images of cell alignment at each flow condition. Pulsatile flow stimulated perpendicular alignment of cell nuclei to the flow, whereas steady flow produced parallel alignment and static culture engendered random alignment. We further measured the alignment angle of nuclei at each condition (Fig. 6c). Under static condition, the alignment angles (43.8° ± 17.7°) were uniformly distributed in the range of 0°–90°, indicating a random orientation. The mean angles of the nuclei were 25° ± 17° for static flow and 68° ± 16° for pulsatile flow, respectively. These results are in good agreement with the previous reports.[40,41] In addition, a higher level of nitric oxide (NO) was released in the perfused TEBV compared to the static culture. Although there is no statistical significance between the two flow conditions (Fig. 6d). Hemodynamic stimuli, such as cyclic stretch and fluid shear stress, would enhance NO production in response to flow by endothelial NO synthase, as observed in this study.[42–44]

We also examined the functional bioactivity of TEBVs following treatment with the vasoconstrictor phenylephrine, which is an α_1-adrenergic receptor agonist acting on vascular smooth muscle.[45] Vasoconstriction in response to 1 μM of phenylephrine was higher under pulsatile stimulation (8.90 ± 0.65%) compared to both steady flow (7.33 ± 0.51%) and static culture (4.13 ± 0.47%) as shown in Fig. 6e. A 0.05 level of significance was shown between the pulsatile and steady flow conditions. Also, the result of steady and static flow condition was statistically significant with *p*-value of less

than 0.001. These results indicate that the pulsatile flow provides a more physiologically mimetic environment to improve the maturation of TEBV.

Conclusion

We have successfully developed a flow control system for microfluidic device using novel tunable valve of magnetoactive sponge, which is easy to fabricate and use at low costs. Under non-uniform magnetic fields, the magnetoactive sponge instantaneously shrinks its volume by collapsing the pores and, therefore, reducing its porosity. The effect of pulsatile flow on the cell alignment was also evaluated. When the pulsatile flow was applied, the nucleus of cell was aligned at an angle of 68° ± 16° whereas 25° ± 17° in static flow. Moreover, pulsatile flow helps to improve TEBV maturation demonstrated by the NO releasing and vasoconstriction tests. As a result, we can instantaneously vary the hydraulic permeability of the sponges on demand by applying magnetic fields. The microfluidic systems with tunable flow patterns are particularly suitable for studying tissues on microfluidic chips by providing physiological environment.

Acknowledgements

The work was supported by UH2TR000505 and the NIH Common Fund for the Microphysiological Systems Initiative. X. Z. acknowledges the supports from NSF (MMI-1253495, CMMI-1200515, and DMR-1121107).

References

1 C. D. Chin, V. Linder and S. K. Sia, *Lab Chip*, 2012, **12**, 2118–2134.
2 S.-B. Huang, S.-S. Wang, C.-H. Hsieh, Y. C. Lin, C.-S. Lai and M.-H. Wu, *Lab Chip*, 2013, **13**, 1133–1143.
3 L. Mazutis, J. Gilbert, W. L. Ung, D. A. Weitz, A. D. Griffiths and J. A. Heyman, *Nat. Protoc.*, 2013, **8**, 870–891.
4 S. Hong, H.-J. Hsu, R. Kaunas and J. Kameoka, *Lab Chip*, 2012, **12**, 3277–3280.
5 S. Hong, P.-H. Tsou, C.-K. Chou, H. Yamaguchi, C. B. Su, M.-C. Hung and J. Kameoka, *Biomicrofluidics*, 2012, **6**, 024132–024138.
6 D. Huh, B. D. Matthews, A. Mammoto, M. Montoya-Zavala, H. Y. Hsin and D. E. Ingber, *Science*, 2010, **328**, 1662–1668.
7 D. Huh, G. A. Hamilton and D. E. Ingber, *Trends Cell Biol.*, 2011, **21**, 745–754.
8 H. J. Kim, D. Huh, G. Hamilton and D. E. Ingber, *Lab Chip*, 2012, **12**, 2165–2174.
9 D. Huh, Y.-S. Torisawa, G. A. Hamilton, H. J. Kim and D. E. Ingber, *Lab Chip*, 2012, **12**, 2156–2164.
10 D. Huh, D. C. Leslie, B. D. Matthews, J. P. Fraser, S. Jurek, G. A. Hamilton, K. S. Thorneloe, M. A. McAlexander and D. E. Ingber, *Sci. Transl. Med.*, 2012, **4**, 159ra147.
11 P. B. Dobrin, *Physiol. Rev.*, 1978, **58**, 397–460.
12 R. Estrada, G. A. Giridharan, M.-D. Nguyen, T. J. Roussel, M. Shakeri, V. Parichehreh, S. D. Prabhu and P. Sethu, *Anal. Chem.*, 2011, **83**, 3170–3177.
13 C. E. Ghezzi, P.-A. Risse, B. Marelli, N. Muja, J. E. Barralet, J. G. Martin and S. N. Nazhat, *Biomaterials*, 2013, **34**, 1954–1966.
14 T. Ziegler, K. Bouzourène, V. J. Harrison, H. R. Brunner and D. Hayoz, *Arterioscler., Thromb., Vasc. Biol.*, 1998, **18**, 686–692.
15 N. Toshihide, T. Ryuji, N. Ichiro, O. Hayato and Y. Hisataka, *Am. J. Physiol.*, 2000, **278**, H1098–H1104.
16 J. H. Haga, Y.-S. J. Li and S. Chien, *J. Biomech.*, 2007, **40**, 947–960.
17 J. W. Song, W. Gu, N. Futai, K. A. Warner, J. E. Nor and S. Takayama, *Anal. Chem.*, 2005, **77**, 3993–3999.
18 T. Vestad, D. W. M. Marr and J. Oakey, *J. Micromech. Microeng.*, 2004, **14**, 1503–1506.
19 P. Tingrui, J. M. Scott, M. K. Eleanor and Z. Babak, *J. Micromech. Microeng.*, 2005, **15**, 1021–1026.
20 C. Yamahata, F. Lacharme, Y. Burri and M. A. M. Gijs, *Sens. Actuators, B*, 2005, **110**, 1–7.
21 E. W. Lam, G. A. Cooksey, B. A. Finlayson and A. Folch, *Appl. Phys. Lett.*, 2006, **89**, 164105.
22 H. A. Stone, *Nat. Phys.*, 2009, **5**, 178–179.
23 H. Chen, J. Cornwell, H. Zhang, T. Lim, R. Resurreccion, T. Port, G. Rosengarten and R. E. Nordon, *Lab Chip*, 2013, **13**, 2999–3007.
24 H. Nakadatey, Y. Hirose, E. Sekizuka and H. Minamitani, *J. Biomech. Sci. Eng.*, 2008, **03**, 25–37.
25 P. J. Lee, T. A. Gaige and P. J. Hung, *Lab Chip*, 2009, **9**, 164–166.
26 X. Zhao, J. Kim, C. A. Cezar, N. Huebsch, K. Lee, K. Bouhadir and D. J. Mooney, *Proc. Natl. Acad. Sci. U. S. A.*, 2010, **108**, 67–72.
27 K. Cha and D. Kim, *Biomed. Microdevices*, 2011, **13**, 877–883.
28 S.-J. Choi, T.-H. Kwon, H. Im, D.-I. Moon, D. J. Baek, M.-L. Seol, J. P. Duarte and Y.-K. Choi, *ACS Appl. Mater. Interfaces*, 2011, **3**, 4552–4556.
29 L. Che-Hsin, L. Gwo-Bin, C. Bao-Wen and C. Guan-Liang, *J. Micromech. Microeng.*, 2002, **12**, 590.
30 T. Ueda, B. L. Gray, Y. Chen and P. Li, *Proc. SPIE*, 2008, **6886**, 68860P-1-68860P-9.
31 S. Jain, H. Xu, H. Duncan, J. W. Jones Jr., J. X. Zhang, M. G. Clemens and C. Y. Lee, *Cryobiology*, 2004, **48**, 322–332.
32 Y. Yang, K. Kulangara, J. Sia, L. Wang and K. W. Leong, *Lab Chip*, 2011, **11**, 1638–1646.
33 S. Das, S. Chakraborty and S. Mitra, *Microfluid. Nanofluid.*, 2012, **13**, 799–807.
34 S. Cook, M. Togni, M. C. Schaub, P. Wenaweser and O. M. Hess, *Eur. Heart J.*, 2006, **27**, 2387–2393.
35 P. M. Doubilet, C. B. Benson and J. S. Chow, *AJR, Am. J. Roentgenol.*, 2000, **175**, 67–69.
36 D. N. Ku, *Annu. Rev. Fluid Mech.*, 1997, **29**, 399–434.
37 S. Spronk, P. T. den Hoed, L. C. W. de Jonge, L. C. van Dijk and P. M. T. Pattynama, *J. Vasc. Surg.*, 2005, **42**, 236–242.

38 S. Q. Liu, D. Tang, C. Tieche and P. K. Alkema, *Am. J. Physiol.*, 2003, **285**, H1072–H1080.
39 S. Q. Liu, C. Tieche, D. Tang and P. K. Alkema, *Am. J. Physiol.*, 2003, **285**, H1081–H1090.
40 A. A. Lee, W. J. Karlon, D. A. Graham, S. Dela Cruz and A. Ratcliffe, *J. Biomech. Eng.*, 2001, **124**, 37–43.
41 K. M. Rice, S. K. Kakarla, S. P. Mupparaju, S. Paturi, A. Katta, M. Wu, R. T. Harris and E. R. Blough, *Biotechnol. Appl. Biochem.*, 2010, **55**, 85–90.
42 M. Dixit, A. E. Loot, A. Mohamed, B. Fisslthaler, C. M. Boulanger, B. Ceacareanu, A. Hassid, R. Busse and I. Fleming, *Circ. Res.*, 2005, **97**, 1236–1244.
43 F. Ingrid and B. Rudi, *Am. J. Physiol.*, 2003, **284**, R1–R12.
44 B. Yong Chool and J. Hanjoong, *Am. J. Physiol.*, 2003, **285**, C499–C508.
45 M. C. Christine, L. Cheng-Han, A. G. Stephanie, M. K. Albert, C. C. Richard and B. Cornelis van, *Am. J. Physiol.*, 2002, **283**, H1271–H1281.

